Inverted Nanocone-Based Thin Film Photovoltaics with Omnidirectionally Enhanced Performance

Qingfeng Lin,[†] Siu-Fung Leung,[†] Linfeng Lu,[‡] Xiaoyuan Chen,[‡] Zhuo Chen,[†] Haoning Tang,[†] Wenjun Su,[§] Dongdong Li,[‡,*] and Zhiyong Fan[†,*]

[†]Department of Electronic and Computer Engineering, The Hong Kong University of Science and Technology, Clear Water Bay, Kowloon, Hong Kong, China, [‡]Shanghai Advanced Research Institute, Chinese Academy of Sciences, 99 Haike Road, Zhangjiang Hi-Tech Park, Pudong, Shanghai 201210, China, and [§]School of Mechanical Engineering, Xi'an Jiaotong University, Xi'an Shaanxi 710049, China

ABSTRACT Thin film photovoltaic (PV) technologies are highly attractive for low-cost solar energy conversion and possess a wide range of potential applications from building-integrated PV generation to portable power sources. Inverted nanocones (i-cones) have been demonstrated as a promising structure for practical thin film PV devices/modules, owning to their antireflection effect, self-cleaning function, superior mechanical robustness, and so forth. In this work, we have demonstrated a low-cost and scalable approach to achieve perfectly ordered i-cone arrays. Thereafter, thin film amorphous silicon (a-Si:H) solar cells have been fabricated based on various i-cone substrates with different aspect ratios and pitches to investigate the impact of geometry of i-cone nanostructures on the performance of the as-obtained PV devices. Intriguingly, the optical property investigations and device performance characterizations demonstrated that the 0.5-aspect-ratio i-cone-based device performed the best on both light absorption capability and energy conversion efficiency, which is 34% higher than that of the flat counterpart. Moreover, the i-cone-based device enhanced the light absorption and device performance over the flat reference device omnidirectionally. These results demonstrate a viable and convenient route toward scalable fabrication of nanostructures for high-performance thin film PV devices based on a broad range of materials.

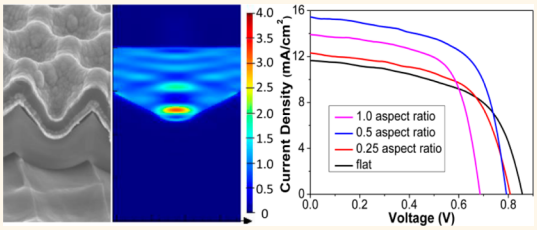

KEYWORDS: thin film photovoltaics · inverted nanocones · low-cost and scalable approach · aspect ratio · light absorption capability · energy conversion efficiency

Photovoltaic (PV) technologies are gaining considerable interest as one set of the most promising technologies for clean and renewable solar energy conversion. Thin film PV technologies are highly attractive for low-cost applications, due to small material usage and low-temperature processes, as compared with the conventional crystalline Si-based PVs. Additionally, lightweight, mechanically flexible thin film solar cells possess a wide range of potential applications from building-integrated PV generation to portable power sources.[1−3] Meanwhile, it is worth pointing out that efficient light absorption is crucial for high-efficiency thin film PV devices, due to the utilization of thin active materials. As such, a variety of three-dimensional nanostructures, such as nanocones,[4−6] nanowires,[7−9] nanopillars,[10−14] nanorods,[15−17] nanopyramids,[18−20] nanospikes,[21−24] nanospheres,[25,26] and nanowells,[27−29] have been extensively studied for improving the performance of thin film PV devices, utilizing various advanced light management schemes.[30−32] Particularly, nanocones have been demonstrated with a promising capability of harvesting sunlight over a large wavelength and incident angle range, due to the gradually tuned effective refractive index.[4−6] Intriguingly, it has been discovered that the inverted nanocones (i-cones) are far superior to nanocones, nanowires, nanopillars, *etc.*, in terms of mechanical robustness due to the redistribution of the normal and shearing mechanical loads.[33] Meanwhile, i-cone nanostructures possess the antireflection effect and self-cleaning function akin to that of nanocones.[4,33,34] These findings suggest that i-cones are excellent structures for high-efficiency thin film solar cells/panels with improved light harvesting capability and reasonable robustness. On the other hand, in order to reach an optimal balance

* Address correspondence to eezfan@ust.hk; lidd@sari.ac.cn.

Received for review May 1, 2014 and accepted May 29, 2014.

Published online 10.1021/nn5023878

between light harvesting and carrier collection, precise geometry control of the utilized nanostructures is the key.[21] However, in the past such a precise geometry control has rarely been demonstrated, and the regular i-cone structures have been mostly fabricated with costly lithographic and etching processes, which limit their practical applications.[33,35] In this work, perfectly ordered i-cone arrays have been achieved with a low-cost and scalable approach. The geometry of the i-cone arrays, *i.e.*, depth and pitch, can be precisely programmed by controlling anodization in conjunction with nanoimprinting. Thereafter, thin film hydrogenated amorphous silicon (a-Si:H) solar cells were fabricated on various i-cone substrates with different aspect ratios and pitches in order to demonstrate the effectiveness of the i-cone nanostructures. Note that the aspect ratio is defined as the ratio between depth and pitch of the i-cone arrays. Both optical and device performances of the i-cone-based thin film a-Si:H solar cells have been investigated. Intriguingly, the optical property investigations and device performance characterizations demonstrated that the 0.5-aspect-ratio i-cone-based device performed the best on both light absorption capability and energy conversion efficiency, which is 34% higher than that of the flat counterpart. Furthermore, the i-cone-based device can enhance the device performance over the flat reference device omnidirectionally, which is beneficial for practical applications. These results demonstrate a viable and convenient route toward scalable fabrication of nanostructures for high-performance thin film PV devices, and the developed i-cone nanostructures can be used for other types of thin film photovoltaics, such as perovskite, copper–indium–gallium-selenide (CIGS) and cadmium telleride (CdTe) solar cells, as the nanostructures can withstand relatively high processing temperatures.

RESULTS AND DISCUSSION

The hexagonally ordered i-cone arrays in this work (Figure 1a1) were fabricated by a low-cost and scalable multistep anodization and wet etching process on the imprinted Al foil in an acidic solution with a proper direct-current (dc) voltage,[36] and the details of the process can be found in the Methods section. Figure 1b1, c1, and d1 show scanning electron microscopy (SEM) images of the 1.5 μm pitch i-cone arrays with aspect ratios of 0.25 (top view), 0.5, and 1.0 (cross-sectional view), respectively. It is worth noting that both the pitch and aspect ratio of the i-cone arrays fabricated *via* this approach are largely tunable, as we have reported recently.[4,36] After obtaining the i-cone arrays, thin film a-Si:H solar cells were fabricated based on them to investigate the influence of geometry of i-cones on the performance of thin film PV devices (Figure 1a2). First, a 100 nm thick Ag layer was sputtered on the i-cone arrays as a back reflector and

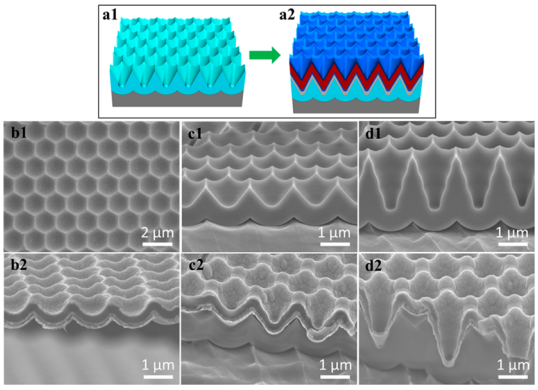

Figure 1. Schematics of i-cones (a1) before and (a2) after thin film a-Si:H device fabrication. SEM images of 1.5 μm pitch i-cone arrays with aspect ratios of (b1) 0.25 (top view), (c1) 0.5 (cross-sectional view), and (d1) 1.0 (cross-sectional view), respectively, before a-Si:H device fabrication. Cross-sectional SEM images of 1.5 μm pitch i-cone arrays with aspect ratios of (b2) 0.25, (c2) 0.5, and (d2) 1.0, respectively, after a-Si:H device fabrication.

bottom electrode, followed by deposition of a 80 nm thick aluminum-doped zinc oxide (AZO) layer as a buffer layer to reduce the metal diffusion into the silicon layer and to diminish undesired parasitic absorption of light in the Ag layer due to excitations of plasmons as well.[35,37] Thereafter, the n-i-p a-Si:H layers were deposited by plasma-enhanced chemical vapor deposition (PECVD) from bottom to top with nominal thicknesses of 30, 280, and 7 nm, respectively, with an 80 nm thick indium tin oxide (ITO) as top electrode. Figure 1b2, c2, and d2 demonstrate cross-sectional SEM images of the as-obtained thin film a-Si:H devices based on 1.5 μm pitch i-cone arrays with aspect ratios of 0.25, 0.5, and 1.0, respectively, from which we can easily observe that 0.25 and 0.5 aspect ratios present excellent film conformality and uniformity on the i-cone substrates, while a 1.0 aspect ratio results in poor film uniformity. Supporting Information Figure S1 shows a photograph of four i-cone devices with 1.5 μm pitch and 0.5 aspect ratio on one Al substrate.

To quantitatively investigate the optical properties of these i-cone nanostructures, UV–vis reflectance spectra were carried out with an integrating sphere.[22] The absorption spectra were achieved by subtracting reflectance from unity, as the devices are opaque. Figure 2a presents the normal incident absorption spectra of the three i-cone devices shown in Figure 1b2, c2, and d2, as well as the flat reference device. It is known that a-Si has an optical band gap of ~1.7 eV, corresponding to a ~720 nm optical wavelength. Therefore, the spectral range 400–720 nm was chosen to investigate above-band-gap optical absorption of these devices. On the other hand, this wavelength range has covered the peak of solar irradiance; thus the results are meaningful for studying the optical properties of the PV devices. Note that the lower boundary of the wavelength range is limited by the home-built measurement setup. As clearly

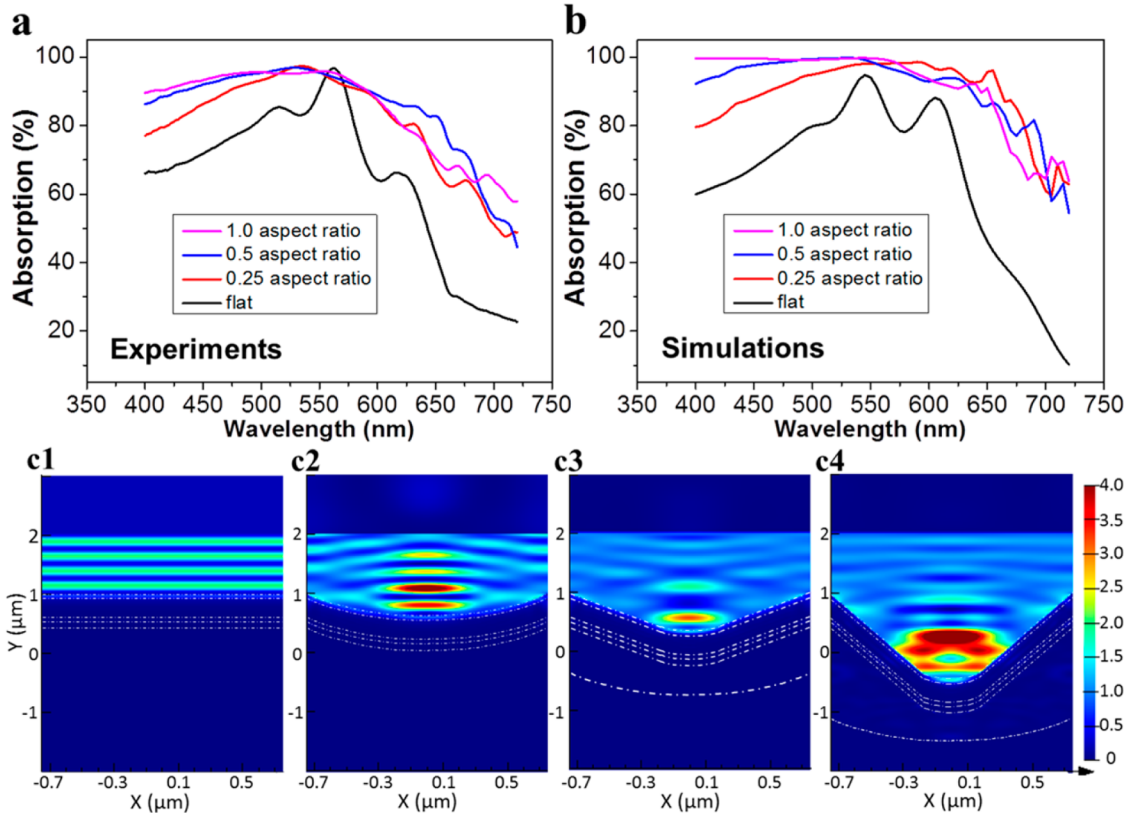

Figure 2. (a) Experimental and (b) simulated absorption spectra of a-Si:H devices based on 1.5 μm pitch i-cone substrates with different aspect ratios and the flat reference. Simulated cross-sectional $|E|^2$ distribution of the EM wave at 500 nm wavelength in a-Si:H devices based on (c1) a flat substrate and 1.5 μm pitch i-cone substrates with aspect ratios of (c2) 0.25, (c3) 0.5, and (c4) 1.0, respectively.

shown in Figure 2a, the 0.25-aspect-ratio device has a much higher absorption capability than the flat device. Furthermore, the 0.5- and 1.0-aspect-ratio devices demonstrated higher broadband absorption than the 0.25-aspect-ratio one. Notably, compared to the 0.5-aspect-ratio device, the 1.0-aspect-ratio device showed slightly higher absorption efficiency over short wavelengths, but lower absorption efficiency over long wavelengths. This is because the 1.0-aspect-ratio i-cone has a superior antireflection property to the 0.5-aspect-ratio one, leading to higher light absorption capability for short wavelengths, where the antireflection effect dominates light absorption. On the other hand, the 1.0-aspect-ratio device has a much thinner a-Si:H layer at the lower part of the i-cones (Figure 1d2), resulting in lower light absorption efficiency over long wavelengths, where the absorption coefficient of a-Si:H is much lower. Consequently, the 0.5-aspect-ratio device presents a slightly higher integrated absorption than the 1.0-aspect-ratio one (Supporting Information Figure S2a) due to the higher photon flux density over longer wavelengths (Supporting Information Figure S2b). Note that the integrated absorption (Supporting Information) presented in this work was obtained by integrating the absorption spectrum with the AM1.5G photon flux spectrum[38] in the wavelength range of 400−720 nm.[10]

In order to further verify the experimental results, finite-difference-time-domain (FDTD) simulations were performed on these devices, resulting in simulated absorption spectra as shown in Figure 2b. Expectedly, the simulated absorption spectra showed a quite consistent trend over all the wavelengths with the experimental ones among these four devices as described above. Moreover, to shed light on how light is coupled into these devices, the cross-sectional electric field intensity ($|E|^2$) distribution of the electromagnetic (EM) wave at 500 nm wavelength was plotted as shown in Figure 2c. In these four simulation models, EM plane waves propagate downward from $Y = 2$ μm and reach the top surfaces of these devices at $Y = 1$ μm. Note that the color index at the specific location in the cross-sectional $|E|^2$ distribution indicates the magnitude of $|E|^2$ at that point, normalized with that of the source EM wave if propagating in free space. The different refractive indexes of the layers of materials in the simulation devices are more clearly illustrated in Supporting Information Figure S3. In order to observe the light propagation in each layer in the devices more easily, white dashed lines were plotted in Figure 2c1−c4 to show the edges of each material in the devices, and the materials were labeled in Supporting Information Figure S3c. Note that there is a thick alumina layer for making 0.5- and 1.0-aspect-ratio i-cones, as shown in

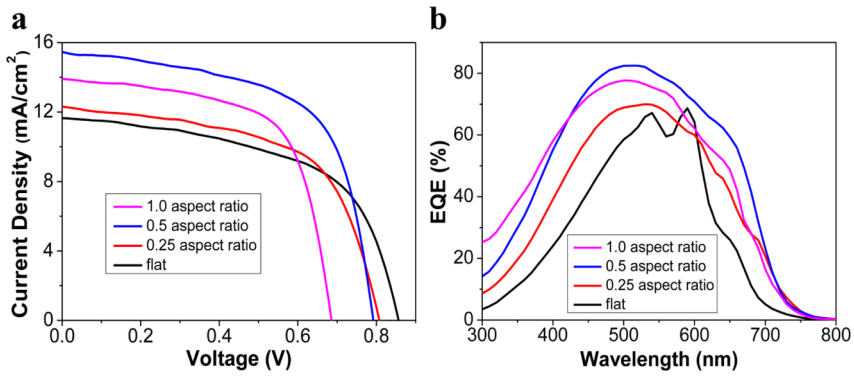

Figure 3. (a) $J-V$ curves and (b) EQE measurements of a-Si:H devices based on 1.5 μm pitch i-cone substrates with different aspect ratios and the flat reference.

Supporting Information Figure S3c and d, but not in Figure S3a and b; detailed information can be found in the Methods section. The fringe patterns in Figure 2c below $Y = 2$ μm originate from the interference between the source light and the reflected light, and the color index above $Y = 2$ μm indicates the intensity of the reflected light. The cross-sectional $|E|^2$ distributions demonstrate a lower reflection for the 0.25-aspect-ratio device (Figure 2c2) than the flat device (Figure 2c1), indicated by the darker color above the light source. Furthermore, the 0.5- and 1.0-aspect-ratio devices (Figure 2c3 and c4) show even lower reflection, which is consistent with the results in Figure 2a and b. Interestingly, the color patterns above $Y = 2$ μm in Figure 2c3 and c4 indicate that the 0.5- and 1.0-aspect-ratio devices have similar reflectance at 500 nm wavelength, while the color patterns below $Y = 1$ μm illustrate that the 1.0-aspect-ratio device has much stronger electric field intensity inside the i-cone nanostructures than the 0.5-apsect-ratio one. This is because more incident photons are coupled into the 1.0-aspect-ratio device due to its superior antireflection effect, and the reflected EM wave from the more inclined sidewall and the bottom of the i-cone yields converge at a location inside the i-cone, akin to the focusing effect inside a concave mirror. In addition, the absorption profiles of these devices in the active layers at 500 nm wavelength are illustrated in Supporting Information Figure S4, demonstrating that most of the light absorption happens in the a-Si:H layer, which is beneficial for electron−hole pair generation and collection.

The above optical investigation shows the potency of i-cone structures for efficient photon capturing. Meanwhile, the device performance of the i-cone-based thin film a-Si:H solar cells was characterized together with the flat reference device. Figure 3a presents current density−voltage ($J-V$) characteristics of the four kinds of devices discussed above with a solar simulator (Newport Corporation, 91150 V) under 1 sun illumination. J_{sc} and V_{oc} extracted from these $J-V$ curves are summarized in Table 1. The $J-V$ curves

TABLE 1. Summary of Device Performances of a-Si:H Solar Cells Based on 1.5 μm Pitch i-Cone Arrays with Different Aspect Ratios and the Flat Reference

device	V_{oc} (V)	J_{sc} (mA/cm^2)	fill factor (%)	efficiency (%)
flat	0.856	11.67	56.7	5.66
0.25 aspect ratio	0.807	12.23	59.4	5.86
0.5 aspect ratio	0.792	15.44	62.0	7.58
1.0 aspect ratio	0.685	13.85	64.4	6.11

demonstrate that the J_{sc} increases significantly from 11.67 mA/cm^2 to 15.44 mA/cm^2 as the aspect ratio increases from 0 (the flat device) to 0.5, attributed to the improved light absorption capability as shown in Figure 2, while it decreases to 13.85 mA/cm^2 when the aspect ratio further increases to 1. The trend for J_{sc} can also be confirmed with external quantum efficiency (EQE) measurements shown in Figure 3b. Meanwhile, it can be seen that V_{oc} decreases monotonically while increasing the aspect ratio from 0 to 0.25, 0.5, and 1.0. The increase of J_{sc} initially can be ascribed to the enhanced light-trapping effect with higher aspect ratio, which has also been observed for other positive nanostructures such as nanopillars and nanospikes.[7,11,21] However, our previous study has shown that, particularly for a-Si:H thin film solar cells, an increase of the structural aspect ratio can lead to a rise of a-Si:H film nonuniformity, which can substantially hurt both J_{sc} and V_{oc} due to the deterioration of the internal electric field and carrier collection capability.[21] Even though the light-trapping effect can compensate the loss on J_{sc}, the loss on V_{oc} typically monotonically depends on the aspect ratio.[21] The nonuniformity of an a-Si:H film on the i-cones can be evidenced in Figure 1d2 and can explain the trend in J_{sc} and V_{oc}. As a result, i-cones with an intermediate aspect ratio of 0.5 present the best overall energy conversion efficiency of 7.58%, as shown in Table 1, which is 34% higher than that of the flat reference device. Note that this overall trend is consistent with what has been discovered for nanopillar/nanospike solar cells,[21] and it clearly suggests that a balance between photon

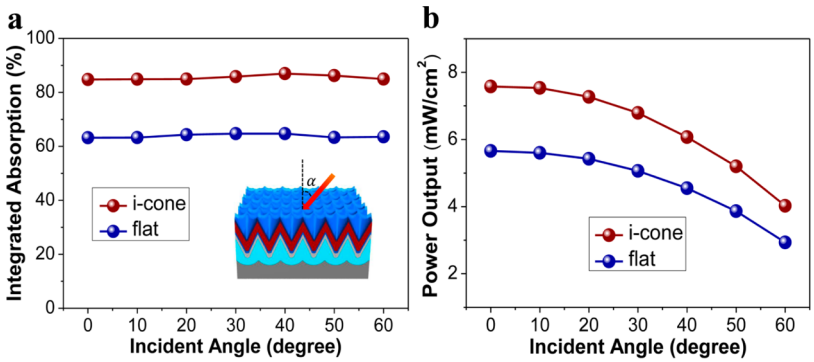

Figure 4. (a) Integrated absorption and (b) power output of the best performance i-cone-based a-Si:H device (based on 1.5 μm pitch 0.5-aspect-ratio i-cones) and the flat reference device.

harvesting and carrier collection is crucial in determining the performance of a nanostructured solar cells. It is worth pointing out that even though the 1.0-aspect-ratio device has rather poor film uniforminty at the lower part of the i-cones (Figure 1d2), its energy conversion efficiency is still higher than that of the flat reference device (Table 1). This is because the 1.0-aspect-ratio i-cone-based device can absorb light much more efficiently than the flat one, and the i-cone arrays are connected by the thicker top portion, where most of the photocarriers can be efficiently collected, even though the films at the lower part of the i-cones are much thinner, since most of the light absorption occurs at the upper part of the nanostructures. This is an important advantage of i-cones over positive nanostructures such as nanopillars, nanodomes, and nanospikes,[21,35] where arrays are connected at the bottom. In addition, the device performances of thin film a-Si:H solar cells based on 1 μm pitch i-cone arrays with aspect ratios of 0.25, 0.5, and 1 were also investigated together with the flat reference device, as shown in Supporting Information Figure S5 and Table S1. Interestingly, the 1 μm pitch i-cone-based PV devices prove similar to the 1.5 μm pitch ones for device performances with respect to the aspect ratio, confirming that the 0.5-aspect-ratio device has the highest energy conversion efficiency. Note that for a particular aspect ratio the 1.5 μm pitch i-cone-based device always has a slightly higher energy conversion efficiency than the 1 μm pitch counterpart, as shown in Table 1 and S1. This is due to the fact for a particular aspect ratio the 1.5 μm pitch one always has slightly better film uniformity than the 1 μm pitch one, which can be observed from Figure 1 and Supporting Information Figure S6.

It is worth pointing out that the above results are based on normal incident light, while for practical operation, the angle of solar irradiation changes over time in a day. Therefore, optical properties and device performances for angular incidences should be investigated. In this regard, we characterized the angular-dependent integrated light absorption and electrical power output of the best performance i-cone-based device, namely, the 1.5 μm pitch 0.5-aspect-ratio device, together with the flat reference device for the sake of comparison. Figure 4a presents the integrated absorption of the i-cone device and flat device for the light incident angles tuning from 0° (normal incident) to 60° with a 10° interval using an integrating sphere and a broadband halogen light source. It can be clearly seen that the i-cone device possesses a much higher integrated absorption than the flat device over all incident angles, with an absolute enhancement of ~20% with small dependence on incident angle. Furthermore, power outputs of these two devices at different incident angles were also measured and plotted in Figure 4b, where the i-cone device demonstrates a substantial improvement of electrical power output over all incident angles compared to the flat counterpart. Overall, the i-cone-based device can enhance the light absorption and power output omnidirectionally, because of the wavelength- and angular-independent antireflection effect of the i-cones due to the gradual change of effective refractive index of the entire nanostructures. The omnidirectional improvement of light absorption and power output is of significance for practical deployment of solar panels without a costly solar tracking system.

CONCLUSION

Inverted nanocones have been demonstrated as a supreme structure for practical thin film PV devices/modules, attributed to their antireflection effect, self-cleaning function, superior mechanical robustness, and so forth. In this work, we have demonstrated a low-cost and scalable approach to achieve perfectly ordered i-cone arrays. Furthermore, thin film a-Si:H solar cells have been fabricated based on various i-cone substrates with different aspect ratios and pitches to investigate the influence of geometry of i-cone nanostructures on the performance of as-obtained PV devices, which has not been reported to our best knowledge. It was found that i-cones with low aspect ratios up to 0.5 present conformal and uniform

deposition of thin film PV device layers, while 1.0-aspect-ratio i-cones have poor film uniformity. Intriguingly, the optical property investigations revealed that the 0.5-aspect-ratio i-cone-based device possessed the best light absorption capability due to the combined antireflection effect and excellent film uniformity. Moreover, the 0.5-aspect-ratio device demonstrated the highest energy conversion efficiency, which is 34% higher than that of the flat reference device. Finally, angular-dependent investigations on optical properties and device performances indicate that i-cone-based thin film PV devices are beneficial for practical applications attributed to the consistent improvement of light absorption and power output over all incident angles. Notably, the i-cone nanostructures presented here can be not only adapted to thin film a-Si:H solar cells but also applied for a wide range of PV technologies based on CIGS, CdTe, perovskite materials, *etc.*, on rigid and flexible substrates. Overall, the i-cones demonstrated here are highly versatile and enable a viable and convenient route to fabricate high-performance thin film PV devices for practical applications.

METHODS

Preparation of i-Cone Arrays. An electrochemically polished clean Al substrate was imprinted using a silicon stamp with hexagonally ordered nanopillars with a height of 200 nm and tunable pitch of 500 nm to 2 μm to produce a nanoindentation array on the surface of the Al substrate. The patterned Al substrate was first anodized with proper conditions to form an ordered alumina channel layer, which was then completely etched away in a mixture of phosphoric acid (6 wt %) and chromic acid (1.8 wt %) at 100 °C, resulting in a 0.25-aspect-ratio Al i-cone substrate. Thereafter, 0.5- and 1.0-aspect-ratio alumina i-cone substrates were achieved by more anodization steps to obtain the desired alumina i-cone depth, in conjunction with wet etching using 5 wt % phosphoric acid (H_3PO_4) at 53 °C between two anodization steps to widen the alumina i-cone pore size, with their fabrication processes (starting from second anodization) shown in Supporting Information Table S2. Note that all the anodization processes were performed in "240 mL, 1:1, 1 wt % citric acid/ethylene glycol + 1.5 mL of 0.1 wt % H_3PO_4" with 600 V at 2 °C for 1.5 μm pitch and "230 mL, 1:1, 4 wt % citric acid/ethylene glycol + 15 mL of 0.1 wt % H_3PO_4" with 400 V at 10 °C for 1 μm pitch.

Fabrication of a-Si:H Solar Cells. A Ag reflector layer was first deposited on the substrate by dc magnetron sputtering at room temperature in an argon plasma atmosphere. Then an AZO spacer layer was prepared by radio frequency (RF) magnetron sputtering of a 2 wt % Al_2O_3-doped ZnO ceramic target (99.99% purity) under argon plasma at a base temperature of 150 °C. Subsequently, a stack of n-i-p a-Si:H layers were successively deposited in a multichamber PECVD system consisting of three PECVD chambers. All these chambers have identical capacitively coupled parallel-plate electrode configurations and serve for the deposition of intrinsic, n-doped, and p-doped layers, respectively. The a-Si:H absorber layers were prepared from a mixture of SiH_4 and H_2 gases at an excitation frequency of 40 MHz. Doping was achieved by gas mixture of hydrogen-diluted phosphine (PH_3) for deposition of the n layer and hydrogen-diluted diborane (B_2H_6) for the p layer at an excitation frequency of 13.56 MHz. After device fabrication, an 80 nm thick ITO layer was deposited by RF sputtering as the top electrode.

Device Characterization. SEM images of the i-cone substrates and i-cone-based thin film a-Si:H PV devices were obtained by a JEOL JSM-6700F SEM working at 5 kV. Angular- and wavelength-dependent absorption spectra of all devices were performed with a home-built ultraviolet/visible measurement system. All the $J-V$ curves of i-cone-based thin film a-Si:H solar cells were carried out using a solar simulator (Newport Corporation, 91150 V) under 1 sun illumination. The EQE measurements were characterized by Oriel QE-PV-SI (Newport Corporation).

Conflict of Interest: The authors declare no competing financial interest.

Acknowledgment. This work was supported by the General Research Fund (612111, 612113) from the Hong Kong Research Grant Council and Hong Kong Innovation and Technology Fund (ITS/117/13) from the Innovation and Technology Commission. We also acknowledge Science & Technology Commission of Shanghai Municipality (Grant No. 13DZ1106000) and the National Natural Science Foundation of China (Grant No. 51102271).

Supporting Information Available: Photograph of i-cone-based thin film a-Si:H solar cells is shown in Figure S1, integrated absorption of a-Si:H solar cells based on 1.5 μm pitch i-cone arrays and the AM1.5G photon flux spectrum are presented in Figure S2, simulation models for a-Si:H devices based on different substrates are illustrated in Figure S3, simulated absorption profiles of a-Si:H devices based on different substrates are illustrated in Figure S4, $J-V$ curves and EQE measurements of a-Si:H devices based on 1 μm pitch i-cone substrates with different aspect ratios and the flat reference are demonstrated in Figure S5, cross-sectional SEM images of a-Si:H devices based on 1 μm pitch i-cones with different aspect ratios are shown in Figure S6, device performances of a-Si:H solar cells based on 1 μm pitch i-cone arrays and the flat reference are summarized in Table S1, and fabrication processes for i-cones with different pitches and aspect ratios are listed in Table S2. This material is available free of charge *via* the Internet at http://pubs.acs.org.

REFERENCES AND NOTES

1. Lin, Q.; Huang, H.; Jing, Y.; Fu, H.; Chang, P.; Li, D.; Yao, Y.; Fan, Z. Flexible Photovoltaic Technologies. *J. Mater. Chem. C* **2014**, *2*, 1233–1247.
2. Fan, Z.; Javey, A. Photovoltaics: Solar Cells on Curtains. *Nat. Mater.* **2008**, *7*, 835–836.
3. Schubert, M. B.; Werner, J. H. Flexible Solar Cells for Clothing. *Mater. Today* **2006**, *9*, 42–50.
4. Tsui, K. H.; Lin, Q.; Chou, H.; Zhang, Q.; Fu, H.; Qi, P.; Fan, Z. Low-Cost, Flexible and Self-Cleaning Three-Dimensional Anti-Reflection Nanocone Arrays for High Efficiency Photovoltaics. *Adv. Mater.* **2014**, *26*, 2805–2811.
5. Jeong, S.; Garnett, E. C.; Wang, S.; Yu, Z.; Fan, S.; Brongersma, M. L.; McGehee, M. D.; Cui, Y. Hybrid Silicon Nanocone-Polymer Solar Cells. *Nano Lett.* **2012**, *12*, 2971–2976.
6. Wang, B.; Leu, P. W. Enhanced Absorption in Silicon Nanocone Arrays for Photovoltaics. *Nanotechnology* **2012**, *23*, 194003.
7. Kelzenberg, M. D.; Boettcher, S. W.; Petykiewicz, J. A.; Turner-Evans, D. B.; Putnam, M. C.; Warren, E. L.; Spurgeon, J. M.; Briggs, R. M.; Lewis, N. S.; Atwater, H. A. Enhanced Absorption and Carrier Collection in Si Wire Array for Photovoltaic Applications. *Nat. Mater.* **2010**, *9*, 239–244.
8. Chang, H.; Lai, K.; Dai, Y.; Wang, H.; Lin, C.; He, J. Nanowire Arrays with Controlled Structure Profiles for Maximizing Optical Collection Efficiency. *Energy Environ. Sci.* **2011**, *4*, 2863–2869.
9. Shin, J. C.; Kim, K. H.; Yu, K. J.; Hu, H.; Yin, L.; Ning, C.; Rogers, J. A.; Zuo, J.; Li, X. In(x)Ga(1-x)as Nanowires on Silicon: One-Dimensional Heterogeneous Epitaxy, Bandgap Engineering, and Photovoltaics. *Nano Lett.* **2011**, *11*, 4831–4838.
10. Lin, Q.; Hua, B.; Leung, S.; Duan, X.; Fan, Z. Efficient Light Absorption with Integrated Nanopillar/Nanowell Arrays

for Three-Dimensional Thin-Film Photovoltaic Applications. *ACS Nano* **2013**, *7*, 2725–2732.
11. Fan, Z. Y.; Razavi, H.; Do, J. W.; Moriwaki, A.; Ergen, O.; Chueh, Y. L.; Leu, P. W.; Ho, J. C.; Takahashi, T.; Reichertz, L. A.; *et al*. Three-Dimensional Nanopillar-Array Photovoltaics on Low-Cost and Flexible Substrate. *Nat. Mater.* **2009**, *8*, 648–653.
12. Fan, Z. Y.; Kapadia, R.; Leu, P. W.; Zhang, X. B.; Chueh, Y. L.; Takei, K.; Yu, K.; Jamshidi, A.; Rathore, A. A.; Ruebusch, D. J.; *et al*. Ordered Arrays of Dual-Diameter Nanopillars for Maximized Optical Absorption. *Nano Lett.* **2010**, *10*, 3823–3827.
13. Kapadia, R.; Fan, Z.; Javey, A. Design Constraints and Guidelines for CdS/CdTe Nanopillar Based Photovoltaics. *Appl. Phys. Lett.* **2010**, *96*, 103116.
14. Kapadia, R.; Fan, Z.; Takei, K.; Javey, A. Nanopillar Photovoltaics: Materials, Processes, and Devices. *Nano Energy* **2012**, *1*, 132–144.
15. Lin, Y.; Lai, K.; Wang, H.; He, J. Slope-Tunable Si Nanorod Arrays with Enhanced Antireflection and Self-Cleaning Properties. *Nanoscale* **2010**, *2*, 2765–2768.
16. Tsai, D.; Lin, C.; Lien, W.; Chang, H.; Wang, Y.; He, J. Ultra-High-Responsivity Broadband Detection of Si Metal–Semiconductor–Metal Schottky Photodetectors Improved by ZnO Nanorod Arrays. *ACS Nano* **2011**, *5*, 7748–7753.
17. Lin, Y.; Wang, H.; Lin, C.; He, J. Surface Profile-Controlled Close-Packed Si Nanorod Arrays for Self-Cleaning Antireflection Coatings. *J. Appl. Phys.* **2009**, *106*, 114310.
18. Chen, H.; Chuang, S.; Lin, C.; Lin, Y. Using Colloidal Lithography to Fabricate and Optimize Sub-Wavelength Pyramidal and Honeycomb Structures in Solar Cells. *Opt. Express* **2007**, *15*, 14793–14803.
19. Han, S. E.; Chen, G. Toward the Lambertian Limit of Light Trapping in Thin Nanostructured Silicon Solar Cells. *Nano Lett.* **2010**, *10*, 4692–4696.
20. Mavrokefalos, A.; Han, S. E.; Yerci, S.; Branham, M. S.; Chen, G. Efficient Light Trapping in Inverted Nanopyramid Thin Crystalline Silicon Membranes for Solar Cell Applications. *Nano Lett.* **2012**, *12*, 2792–2796.
21. Leung, S.; Gu, L.; Zhang, Q.; Tsui, K.; Shieh, J.; Shen, C.; Hsiao, T.; Hsu, C.; Lu, L.; Li, D.; *et al*. Roll-to-Roll Fabrication of Large Scale and Regular Arrays of Three-Dimensional Nanospikes for High Efficiency and Flexible Photovoltaics. *Sci. Rep.* **2014**, *4*, 4243.
22. Yu, R.; Ching, K.; Lin, Q.; Leung, S.; Arcrossito, D.; Fan, Z. Strong Light Absorption of Self-Organized 3-D Nanospike Arrays for Photovoltaic Applications. *ACS Nano* **2011**, *5*, 9291–9298.
23. Liao, Y.; Wang, Y.; Yen, Y.; Chen, C.; Hsieh, D.; Chen, S.; Lee, C.; Lai, C.; Kuo, W.; Juang, J. Non-Antireflective Scheme for Efficiency Enhancement of Cu (in, Ga) Se2 Nanotip Array Solar Cells. *ACS Nano* **2013**, *7*, 7318–7329.
24. Lin, H.; Xiu, F.; Fang, M.; Yip, S.; Cheung, H.; Wang, F.; Han, N.; Chan, K. S.; Wong, C.; Ho, J. C. Rational Design of Inverted Nanopencil Arrays for Cost-Effective, Broadband and Omnidirectional Light Harvesting. *ACS Nano* **2014**, *8*, 3752–3760.
25. Yao, Y.; Yao, J.; Narasimhan, V. K.; Ruan, Z.; Xie, C.; Fan, S.; Cui, Y. Broadband Light Management Using Low-Q Whispering Gallery Modes in Spherical Nanoshells. *Nat. Commun.* **2012**, *3*, 664.
26. Grandidier, J.; Callahan, D. M.; Munday, J. N.; Atwater, H. A. Light Absorption Enhancement in Thin-Film Solar Cells Using Whispering Gallery Modes in Dielectric Nanospheres. *Adv. Mater.* **2011**, *23*, 1272–1276.
27. Leung, S. F.; Yu, M.; Lin, Q.; Kwon, K.; Ching, K. L.; Gu, L.; Yu, K.; Fan, Z. Efficient Photon Capturing with Ordered Three-Dimensional Nanowell Arrays. *Nano Lett.* **2012**, *12*, 3682–3689.
28. Han, S. E.; Chen, G. Optical Absorption Enhancement in Silicon Nanohole Arrays for Solar Photovoltaics. *Nano Lett.* **2010**, *10*, 1012–1015.
29. Peng, K.; Wang, X.; Li, L.; Wu, X.; Lee, S. High-Performance Silicon Nanohole Solar Cells. *J. Am. Chem. Soc.* **2010**, *132*, 6872–6873.
30. Leung, S.; Zhang, Q.; Xiu, F.; Yu, D.; Ho, J. C.; Li, D.; Fan, Z. Light Management with Nanostructures for Optoelectronic Devices. *J. Phys. Chem. Lett.* **2014**, *5*, 1479–1495.
31. Hua, B.; Lin, Q.; Zhang, Q.; Fan, Z. Efficient Photon Management with Nanostructures for Photovoltaics. *Nanoscale* **2013**, *5*, 6627–6640.
32. Yu, R.; Lin, Q.; Leung, S. F.; Fan, Z. Nanomaterials and Nanostructures for Efficient Light Absorption and Photovoltaics. *Nano Energy* **2012**, *1*, 57–72.
33. Kim, J.; Choi, H. J.; Park, K.; Cohen, R. E.; McKinley, G. H.; Barbastathis, G. Multifunctional Inverted Nanocone Arrays for Non-Wetting, Self-Cleaning Transparent Surface with High Mechanical Robustness. *Small* **2014**, 10.1002/smll.201303051.
34. Zhu, J.; Hsu, C.; Yu, Z.; Fan, S.; Cui, Y. Nanodome Solar Cells with Efficient Light Management and Self-Cleaning. *Nano Lett.* **2010**, *10*, 1979–1984.
35. Hsu, C. M.; Battaglia, C.; Pahud, C.; Ruan, Z.; Haug, F. J.; Fan, S.; Ballif, C.; Cui, Y. High-Efficiency Amorphous Silicon Solar Cell on a Periodic Nanocone Back Reflector. *Adv. Energy Mater.* **2012**, *2*, 628–633.
36. Lin, Q.; Leung, S.; Tsui, K.; Hua, B.; Fan, Z. Programmable Nanoengineering Templates for Fabrication of Three-Dimensional Nanophotonic Structures. *Nanoscale Res. Lett.* **2013**, *8*, 268.
37. Huang, H.; Lu, L.; Wang, J.; Yang, J.; Leung, S.; Wang, Y.; Chen, D.; Chen, X.; Shen, G.; Li, D. D.; *et al*. Performance Enhancement of Thin-Film Amorphous Silicon Solar Cells with Low Cost Nanodent Plasmonic Substrates. *Energy Environ. Sci.* **2013**, *6*, 2965–2971.
38. Air Mass 1.5 Spectra. American Society for Testing and Materials: West Conshohocken, PA, http://rredc.nrel.gov/solar/spectra/am1.5/.